

Influence of process parameters on surface roughness of aluminum parts produced by DMLS

*Original*

Influence of process parameters on surface roughness of aluminum parts produced by DMLS / Calignano, F.; Manfredi, D.; Ambrosio, E. P.; Iuliano, Luca; Fino, Paolo. - In: INTERNATIONAL JOURNAL, ADVANCED MANUFACTURING TECHNOLOGY. - ISSN 0268-3768. - ELETTRONICO. - 67:9-12(2013), pp. 2743-2751. [10.1007/s00170-012-4688-9]

*Availability:*

This version is available at: 11583/2505584 since: 2016-09-09T14:17:29Z

*Publisher:*

Springer Verlag Germany

*Published*

DOI:10.1007/s00170-012-4688-9

*Terms of use:*

This article is made available under terms and conditions as specified in the corresponding bibliographic description in the repository

*Publisher copyright*

(Article begins on next page)

# Influence of process parameters on surface roughness of aluminum parts produced by DMLS

F. Calignano · D. Manfredi · E. P. Ambrosio · L. Iuliano · P. Fino

**Abstract** Direct metal laser sintering (DMLS) is an additive manufacturing technique for the fabrication of near net-shaped parts directly from computer-aided design data by melting together different layers with the help of a laser source. This paper presents an investigation of the surface roughness of aluminum samples produced by DMLS. A model based on an  $L_{18}$  orthogonal array of Taguchi design was created to perform experimental planning. Some input parameters, namely laser power, scan speed, and hatching distance were selected for the investigation. The upper surfaces of the samples were analyzed before and after shot peening. The morphology was analyzed by means of field emission scanning electron microscope. Scan speed was found to have the greatest influence on the surface roughness. Further, shot peening can effectively reduce the surface roughness.

**Keywords** Aluminum AlSi10Mg · Direct metal laser sintering (DMLS) · Taguchi method · Surface roughness

## Abbreviations

AM	Additive manufacturing
DMLS	Direct metal laser sintering
CAD	Computer-aided design

---

F. Calignano (✉) · D. Manfredi · E. P. Ambrosio · P. Fino  
Center for Space Human Robotics IIT@Polito,  
Istituto Italiano di Tecnologia, Corso Trento, 21,  
10129 Turin, Italy  
e-mail: flaviana.calgiano@iit.it

L. Iuliano  
DIGEP—Dipartimento di Ingegneria Gestionale e della  
Produzione, Politecnico di Torino, Corso Duca degli Abruzzi 24,  
10129 Turin, Italy

P. Fino  
DISAT—Dipartimento Scienza Applicata e Tecnologia,  
Politecnico di Torino, Corso Duca degli Abruzzi 24,  
10129 Turin, Italy

SFF	Solid freeform fabrication
FFEs	Fractional factorial experiments
SLS	Selective laser sintering
S/N	Signal to noise ratio
ANOVA	Analysis of variance
FESEM	Field emission scanning electron microscope
BO	Beam offset

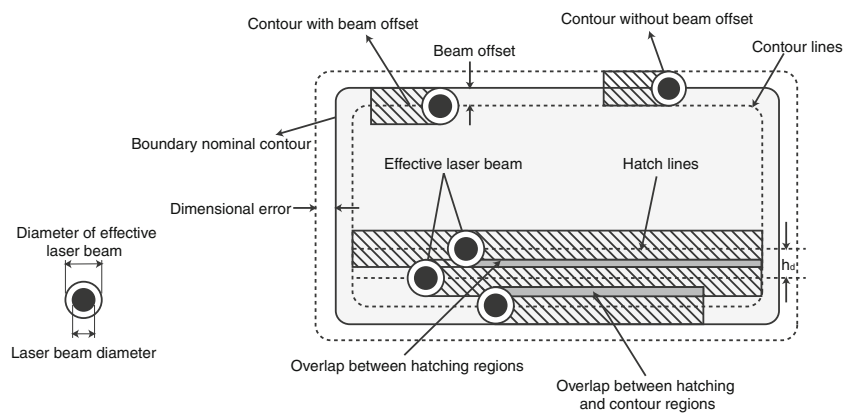
## Nomenclature

$V$	Scan speed (millimeter per second)
$P$	Laser power (watt)
$h_d$	Hatching distance (millimeter)
$E$	Energy density (joule per square millimeter)
$\eta_L$	S/N calculated for larger-the-better response
$\eta_S$	S/N calculated for smaller-the-better response
$R_a$	Surface roughness (micrometer)

## 1 Introduction

Additive manufacturing (AM) is the “process of joining materials to make objects from 3D model data, usually layer upon layer” [1]. Therefore, AM makes it possible to build parts with very complex geometries directly from computer-aided design (CAD) models without any sort of tools or fixtures and without producing any waste material. Recently, demands for the direct manufacture of full-functional engineering metal components in different industry sectors such as motor racing, aerospace, pneumatics, automotive, and functional prototypes have increased greatly. One of the main SFF processes employed in AM is selective laser sintering (SLS). In this process, a part is built up layer by layer through the consolidation of powder particles with a focused laser beam that selectively scans the surface of the powder bed. Consolidation occurs either by actual fusion of the powder particles or by diffusion bonding. Laser sintering has been utilized to build parts from polymeric materials like

**Fig. 1** Exposure strategies and process parameters



styrene, nylon, glass-filled nylon, and polycarbonate plastics and metallic materials like low-carbon steels, stainless steels, copper, and superalloys [2–10]. However, production of metallic objects by SLS is much more complicated and has been pursued through two different approaches, known as indirect and direct laser sintering [11, 12]. Indirect laser sintering involves the sintering of metal powders either mixed with a binder or coated with a polymer. Hence, powder particles are consolidated by the melting and binding capacity of low melting point polymers, which are eventually burnt off. The part is subsequently infiltrated with a low melting point metal [13–15]. In direct laser sintering, high-density objects are created by the sintering of metal powders, recently also reactive materials like titanium and aluminum, without the aid of a binder [16–18]. Research in recent years has identified the potential of this process to build metallic components that can act as functional prototypes. In fact, with the proper choice of input conditions, direct laser sintering, generally known as direct metal laser sintering (DMLS) can build full dense parts with mechanical properties equivalent or closely resembling those of parts produced by conventional manufacturing. Due to its versatility of materials and shapes, the main advantage of DMLS is to produce metal complex-shaped components in one step, but it also has drawbacks that require careful process control: the high temperature gradients and densification ratio during the process yield high internal stresses or part distortion; the risk of balling and dross formation in the melt pool may result in bad surface roughness (from 8 to 20  $\mu\text{m}$  without any posttreatment) [2, 19, 20]. The surface finish of a part, defined as the irregularities of any material resulting from

machining operations, is critical in many applications, for example those requiring a surface roughness of 0.8  $\mu\text{m}$  or better to avoid premature failure from surface initiated cracking [21]. There is no standard method to enhance the surface quality due to the complex nature of the process and to the different properties of the materials used [19, 22]. Several attempts have been made to model the surface roughness of AM parts. Song [23] investigated the effect of different parameters, such as laser power, spot size, scanning speed, hatching distance, and layer thickness on laser-sintered CuSn-made parts. A generic algorithm to determine the best part orientation was presented by Masood et al. [24] in order to create laser-sintered parts with a higher level of accuracy and surface finish. Byun and Lee [25] found the optimal buildup direction of a rapid prototyping part for different systems. Ning et al. [26] developed a model based on a feed-forward neural network with a back-propagation learning algorithm to improve mechanical properties, accuracy, processing time, and surface roughness for the DMLS process. Delgado et al. [19] investigated the effects of scan speed, layer thickness, and building direction on dimensional error, surface roughness, and mechanical properties of the iron-based materials for DMLS and selective laser melting (SLM). Spierings et al. [27] analyzed the influence of the particle size distribution on surface quality of metallic powders of a part produced by SLM.

It is evident from the literature that there are a number of input parameters that can be controlled and varied so as to get desirable surface quality of the parts. Laser power determines the severity of the temperature gradient, and due to

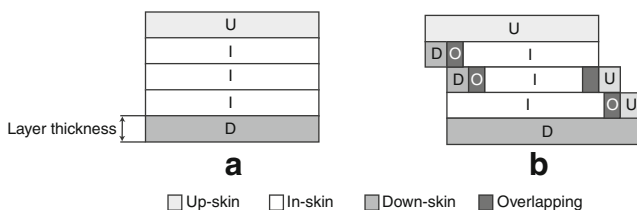


**Fig. 2** Up-down-skin option: **a** exposure without overlapping and **b** exposure with overlapping

**Table 1** Default values of scan speed, laser power and hatching distance for EOS M270 Xtented

Parameters	In-skin (core)	Up-skin (3 layers)	Down-skin (2 layers)	Contour
Scan speed ( $v$ )	800 mm/s	1,000 mm/s	900 mm/s	900 mm/s
Laser power ( $P$ )	195 W	195 W	190 W	80 W
Hatching distance ( $h_d$ )	0.17 mm	0.2 mm	0.1 mm	

**Table 2** Process parameters values for the up-skin

Variable		Fixed	
Parameters	Values	Parameters	Values
$v$ (mm/s)	800, 850, 900, 950, 1,000, 1,250	Layer thickness ( $\mu\text{m}$ )	30
$P$ (W)	120, 155, 190	Spot size (mm)	0.1
$h_d$ (mm)	0.10, 0.15, 0.20		

this temperature rise, sintering of the powder takes place. Hence, the level of power has a significant effect on the surface quality. Scan speed also decides the amount of energy input during the sintering and hence contributes towards the surface quality of the part. Orientation and layer thickness cause stair stepping in DMLS parts, which leads to bad surface finish. Hatch distance has also been found to affect the surface roughness of the DMLS prototypes. The classical methods of experimental planning, e.g., factorial designs, can be used to investigate the influence of some process parameters on surface quality. When the number of factors and levels in each factor increases, application of a full-factorial design is very time consuming, expensive, and sometimes impossible. To minimize the number of tests required, fractional factorial experiments (FFEs) were developed. FFEs use only a portion of the total possible combinations to estimate the effects of the main factors, as well as some of the interactions. Taguchi [28] developed a family of FFE matrices (an orthogonal array) that has generally been adopted to optimize the design parameters and significantly minimize the overall testing time and experimental costs following a systematic approach to confine the number of experiments and tests [29, 30].

The primary aim of the present investigation was to study the DMLS of AlSi10Mg powder through statistically designed experiments based on an  $L_{18}$  orthogonal array of Taguchi design in order to determine the significance of the process parameters affecting the quality of the sintered parts with respect to surface roughness. In fact in literature there is still little detailed information regarding the aluminum parts produced by DMLS process. The signal to noise (S/N) ratio and the analysis of variance (ANOVA) were used to analyze the results. A mathematical model was developed relating the significant process parameters to the output response. Samples were investigated on top surfaces before and after shot peening. Moreover, samples were analyzed by means of field emission scanning electron microscope (FESEM).

**Table 3** Nominal composition of EOS AlSi10Mg alloy powder in accordance with standard DIN EN 1706:2010-06

Element	Si	Fe	Cu	Mn	Mg	Zn	Ti	Al
Weight %	9–11	$\leq 0.55$	$\leq 0.05$	$\leq 0.45$	0.2–0.45	$\leq 0.1$	$\leq 0.15$	Remainder

**Table 4** Combination of control parameters based on  $L_{18}$  array, results of experiment and S/N ratios

Number samples	$v$ (mm/s)	$P$ (W)	$h_d$ (mm)	$E$ (J/mm <sup>2</sup> )	$R_a$ ( $\mu\text{m}$ )	S/N ratios (dB)
1	800	120	0.15	1.00	17.61	-24.92
2	800	155	0.20	0.97	20.46	-26.22
3	800	190	0.10	2.38	14.35	-23.14
4	850	120	0.20	0.71	17.11	-24.67
5	850	155	0.10	1.82	21.39	-26.60
6	850	190	0.15	1.49	21.52	-26.66
7	900	120	0.15	0.89	16.01	-24.09
8	900	155	0.20	0.86	16.57	-24.39
9	900	190	0.10	2.11	15.11	-23.59
10	950	120	0.20	0.63	17.62	-24.92
11	950	155	0.10	1.63	15.57	-23.85
12	950	190	0.15	1.33	17.50	-24.86
13	1,000	120	0.10	1.20	19.59	-25.84
14	1,000	155	0.15	1.03	24.71	-27.86
15	1,000	190	0.20	0.95	23.97	-27.59
16	1,250	120	0.10	0.96	18.14	-25.17
17	1,250	155	0.15	0.83	23.93	-27.58
18	1,250	190	0.20	0.76	22.19	-26.92

## 2 DMLS process

### 2.1 Exposure strategies and process parameters

In the direct metal laser sintering process, a moving laser source with a fixed scan value ( $v$ ) selectively sinters each layer of powder material line by line. The diameter of the region where the particles are sintered (effective sintering range) is larger than the physical beam diameter. This range is denoted as the effective diameter of the laser beam (Fig. 1), which is proportional to the laser power and in-versely proportional to the scanning speed of the laser.

In order to compensate for the dimensional error due to spot diameter, the laser beam should be shifted by half the curing width from the contour to the inside [31]. This correction of the position is called beam offset (BO). The BO value is again defined with respect to the edge of the boundary, and if this value is higher or lower than the correct value, powder outside the layer edge could be sintered or part of the intended edge region might not be sintered, which would disrupt the dimensional accuracy of the part (Fig. 1). At the actual exposure, first of all the contour of the layer structure is exposed

with the contour speed and the laser power. After the contour exposure, all of the inner area is solidified. During hatching, the laser beam moves line after line several times. The distance between the lines is called hatching distance ( $h_d$ ) and it is set at about a quarter at the diameter of the laser beam (Fig. 1). If the distance between two adjacent scan lines is larger than the diameter of the laser beam, the metal powders do not bond together well. A large hatch density often brings about high mechanical strength because more energy is absorbed by the metal powder. When the whole inner area is solidified, a second exposure of the exterior part contour is carried out. Here, the contour compensation of the laser is set at an exact value to make sure that the part edges correspond exactly to the CAD data and that parts can thus be built with the correct dimension. This second contour exposure offers two essential advantages [32]. Firstly, sharper part contours are generated with higher temperature gradients because of the higher heat conductivity of the already solidified material in the area of the first contour. On these part contours, the roughness of the vertical planes decreases. Secondly, as the material has already shrunk at the exposure of the first contour and the inner area in the  $x$ - $y$  direction, the second exposure creates a contour that corresponds exactly to the CAD data. The building process accuracy is thus increased. Another important parameter that can lead to a distorted part or to a process interruption is layer thickness. If the value is too high, no optimal adhesion between the single layers can be realized because the curing depth is insufficient. Furthermore, mechanical tension can be generated through this layer which can lead to detachment of the layer below. If the selected value is smaller, a structure can be torn off during the recoating process, as the recoater blade near hit the sintered particles. Laser parameters like laser beam power and spot size and process parameters like scanning speed, hatching distance, and layer thickness have a great influence on the quality of the laser-sintered samples. The range of various process parameters depends on the materials and specification of machine. For a good surface quality, a better understanding and knowledge of these process parameters is needed.

## 2.2 Aluminum samples

The aluminum samples have been prepared by DMLS with an EOSINT M270 Xtended version. In this machine, a powerful ytterbium (Yb) fiber laser system in an argon atmosphere is used to melt powders with a continuous power up to 200 W, a scanning rate up to 7 m/s, and a spot size of 100  $\mu\text{m}$ . The area on the part layer, above which there is no area to be exposed, is called up-skin. The area on part layer, below which there is no exposed area, is called down-skin (Fig. 2). An area is termed as in-skin, where there is above and below exposed areas as shown in Fig. 2a. Different parameters can be assigned for these areas (Table 1). Some overlapping area between in-skin

**Table 5** Analysis of variance for S/N ratios,  $R^2=88.7\%$

Source	$df$	Sum of squares	$F$	$p$	Statistical significance
Scan speed	5	22.671	8.75	0.004	Highly significant
Laser power	2	3.965	3.82	0.068	Significant
Hatching distance	2	5.804	5.60	0.030	Significant
Residual error	8	4.147			
Total	17	36.586			

and up-down-skin area can also be assigned for improved joint among these areas (Fig. 2b).

## 3 Taguchi method, design of experiment, and experimental details

### 3.1 Taguchi method

Taguchi method [28] is based on orthogonal array experiments which provide more reduced variance for the experiment with optimum settings of control parameters. S/N ratios are log functions used as objective functions for optimization, help in data analysis and prediction of optimum results. S/N ratios are calculated using Eq. 1 or Eq. 2 in the case of larger-the-better or smaller-the-better problems, respectively:

$$\eta_L = -10 \log_{10} \left[ (1/n) \sum (1/y_i^2) \right] [\text{dB}] \quad (1)$$

$$\eta_S = -10 \log_{10} \left[ (1/n) \sum y_i^2 \right] [\text{dB}] \quad (2)$$

where  $\eta_L$  (or  $\eta_S$ ) denotes the S/N ratio calculated from observed values,  $y_i$  represents the experimental observed value of the  $i$ th experiment, and  $n$  is the number of repetition of each experiment.

**Table 6** Average S/N ratios

Level	Smaller-the-better—S/N (dB)		
	Scan speed	Laser power	Hatching distance
1	-24.76	-24.93	-24.70
2	-25.98	-26.08	-25.99
3	-24.02	-25.46	-25.78
4	-24.54		
5	-27.10		
6	-26.56		
Delta	3.08	1.15	1.30
Rank	1	3	2

**Table 7** Process setups optimizing response (min  $R_a$ ), predicted (Taguchi) and experimental values

Control factors			Predicted value		Experimental value	
$v$ (mm/s)	$P$ (W)	$h_d$ (mm)	Response value $R_a$ ( $\mu\text{m}$ )	S/N (dB)	Response value $R_a$ ( $\mu\text{m}$ )	S/N (dB)
900	120	0.10	16.65	-22.67	15.68	-23.91

### 3.2 Design of experiment

The three input or control factors chosen for up-skin were scan speed ( $v$ ), studied at six levels, laser power ( $P$ ), and hatching distance ( $h_d$ ) kept at three levels (Table 2). With respect to traditional full-factorial experimental plan, which would require in this case 54 tests, the Taguchi method reduces the number of experiments down to 18. Therefore, the experimental scheme was designed based on an  $L_{18}$  orthogonal array of Taguchi technique with 17 degrees of freedom. ANOVA was then applied to calculate the statistical confidence associated with the drawn conclusions.

### 3.3 Experimental details

Commercial aluminum alloys, AlSi10Mg, purchased by EOS were employed. The available information on the composition of EOS Aluminum was reported in Table 3 as stated by the producer in his data sheets. Samples dimension were  $20 \times 20 \times 5$  mm.

The surface roughness on top surface of sample was measured with the use of Mahr Perthometer M1 before and after shot peening: to compare the different DMLS samples, the average value of the ordinates from centerline, defined as  $R_a$ , was used. It is theoretically derived as the arithmetic average value of departure of the profile from the mean line along a sampling length. The shot peening process was performed with glass microspheres using a sandblasting machine, SD9 Northblast, in order to improve their surface finishing. The samples, before and after shot peening, were also characterized by a FESEM Zeiss SupraTM 40.

## 4 Experimental results and discussion

The objective of experiment was to optimize the process parameters of up-skin in DMLS process to get better (i.e., low value) surface roughness. Therefore, smaller-the-better problem was used. Linear model analysis provides the coefficients for each factor at the low level, their  $p$  values, and an analysis of variance table. For S/N ratios, all the factors and the interaction terms are significant at an  $\alpha$  level of 0.10. The  $R_a$  values measured from the experiments and the S/N ratio values were listed in Table 4. Whether S/N is a negative or positive, number depends on whether mean-squared deviation is a number greater or smaller than 1. In order to produce a good functional sintered part, it is important that the powder on the part bed surface receives a sufficient amount of energy through the laser sintering process. For this reason, the energy density,  $E$ , is calculated by using the following equation [8]:

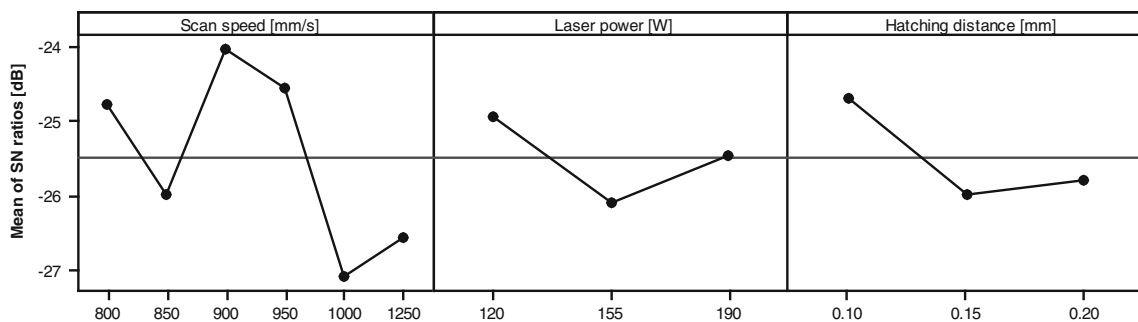
$$E = P / (h_d \times v) \text{ (J/mm}^2\text{)} \quad (3)$$

where  $P$  is the laser power,  $v$  is the scan speed and  $h_d$  is the hatching distance.

### 4.1 Surface roughness

Table 5 shows the analysis of variance for S/N ratios. All factors are significant because its  $p$  value is less than 0.10.

The response table (Table 6) shows the average of each response characteristic (S/N ratios) for each level of each factor. The table includes ranks based on Delta statistics which compare the relative magnitude of effects. The Delta statistic is the highest minus the lowest average for each factor. Rank 1 is assigned to the highest Delta value, rank 2

**Fig. 3** Main effect plot for S/N ratios for  $R_a$

to the second highest, and so on. The level averages in the response table were used to determine which level of each factor provides the best result. As can be seen in the Table 7, scan speed has the greatest influence, followed by hatching distance and laser power.

The main effect plot for S/N ratios for  $R_a$  confirms these results. The plot displays the response means for each factor level. A horizontal line is drawn at the grand mean. The slope of the line which connects the levels of the process variables shows the power of influence of each variable. As seen in Fig. 3, the optimum surface roughness was achieved when the scan speed is 900 mm/s, the laser power is 120 W, and the hatching distance is 0.10 mm. The effects between variables can be visualized with interaction plot (Fig. 4).

Parallel lines in an interactions plot indicate no interaction. The greater the departure of the lines from the parallel state, the higher the degree of interaction. The graph shows that it is possible to obtain low  $R_a$  using low values of scan speed and low values of hatching distance and there are strong interactions between laser power and hatching distance. There is a stronger effect for values of scan speed of 1,250 and 1,000 mm/s when laser power is less than 155 W. There is also a stronger interaction between the scan speed of 800 mm/s and a laser power greater than 155 W. According to Eq.3, increasing laser power and/or decreasing scan speed increases the energy density and therefore the temperature of the powder. When the laser moves, there is a temperature gradient between the laser beam and the solidifying zone; this generates a shear force on the liquid surface that is contrasted by surface tension forces [33]. On one side, low scan speeds improve the top surface finish giving to the so-called melt pools more time to flatten before solidification, by gravity and surface curvature forces that counteract the external shear forces. On the other side, a too low scan speed could increase the volume of liquid produced within the melt pool: this has a tendency to widen the same melt pool provoking a larger

Fig. 4 Interaction plot for  $R_a$

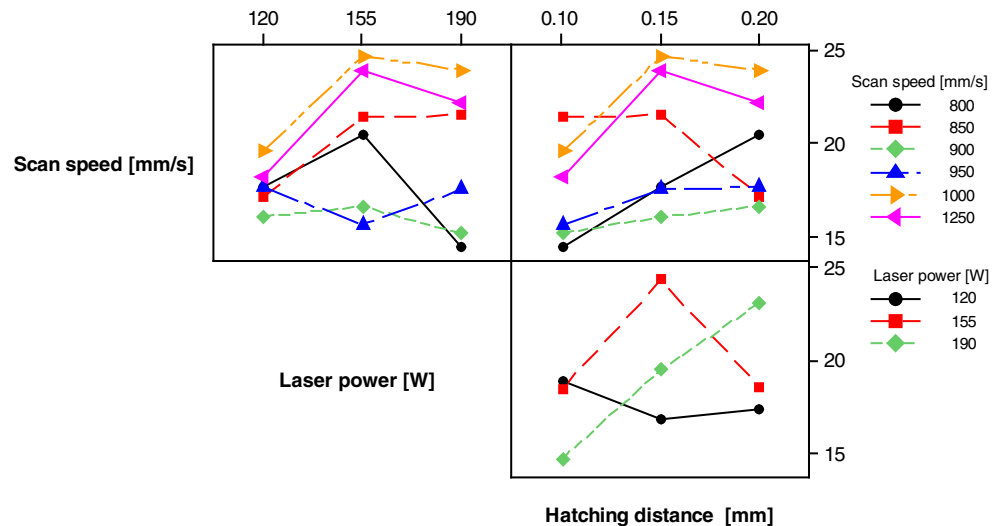


Table 8  $R_a$  after shot peening

Sample	$R_a$ —as built ( $\mu\text{m}$ )	Pressure (bar)	$R_a$ —after shot peening ( $\mu\text{m}$ )	Reduction (%)
15	23.95	4	13.78	43
		6	7.92	67
		8	5.85	76
3	14.35	4	10.08	30
		6	6.95	52
		8	2.50	83

thermal difference across it and consequently a greater variation of surface tensions. Attempting to reduce these changes, the melt pool may break off into smaller entities, well known as “balling,” which solidify at the edge of the melt pool increasing surface roughness. Considering laser power, higher values can flatten the melt pool improving interlayer connection and increasing the wettability of the melt. Improved wettability reduces the melt pool tendency to undergo balling by relieving surface tension variations. However, if these values become too high, large amounts of material vaporization can occur with recoil pressures that disrupt the melt pool surface and increase again the top  $R_a$  [34].

#### 4.2 Regression analysis

A mathematical model of the relation between process parameters and  $R_a$  was developed by regression analysis on the basis of  $L_{18}$  orthogonal array of robust design. Based on the previous analysis, the response equation was developed considering the effects of  $v$ ,  $P$ , and  $h_d$ . The following mathematical model was developed (Eq.4):

$$R_a[\mu\text{m}] = 3.47 + 0.00939v + 0.0201P + 22.9h_d [R^2 = 70.2\%] \quad (4)$$

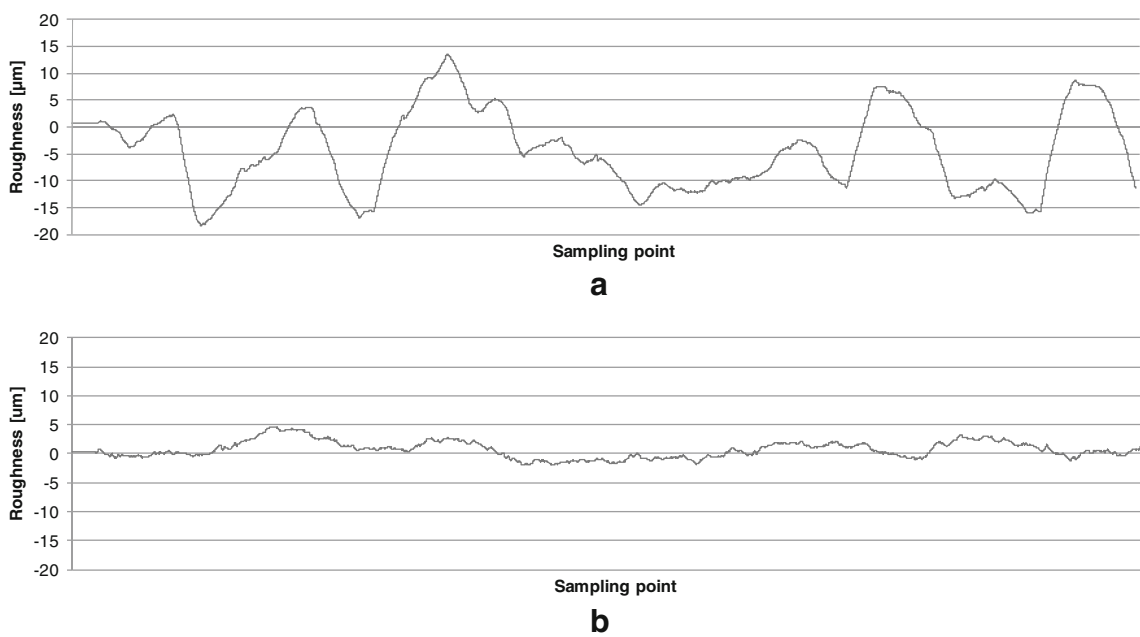


**Fig. 5** Roughness profile of the sample 3 **a** before and **b** after shot peening at 8 bar

The analysis of residuals (differences between the observed and the corresponding fitted values) versus the fitted values shows a nice horizontal band around the residual line (value 0), suggesting the models fit the data well.

#### 4.3 Optimization

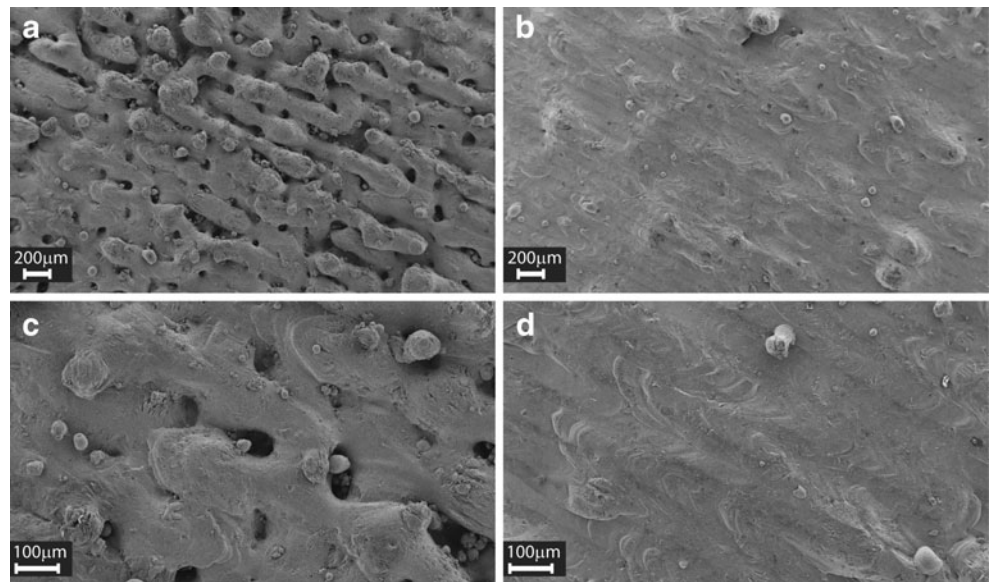
From the analysis of S/N ratio curves, the parameter combinations for AlSi10Mg parts produced by DMLS were obtained that optimize the response: smoothest surface finish, i.e., minimum  $R_a$ . These setups were summarized in

Table 7, together with S/N values predicted by Taguchi analysis compared to experimental ones.

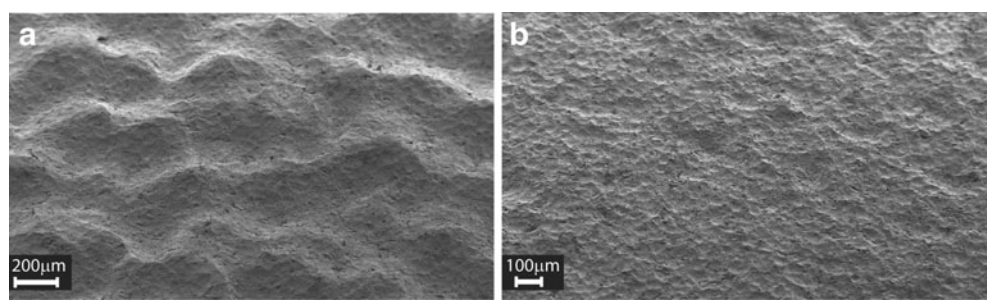
#### 4.4 Shot peening

Shot peening is a cold working process in which the surface of a part is bombarded with small spherical media called shot. Peening with steel shot or glass beads retards the cyclic fatigue failures by inducing compressive stresses on the metal surface and makes it possible to significantly reduce the surface roughness. Glass beads peening produces a

**Fig. 6** FESEM images of surface roughness of sample 15 (**a, c**), built with parameters close to the default ones for up-skin, and of sample 3 (**b, d**)



**Fig. 7** FESEM images of surface roughness of sample 15 (a) and sample 3 (b) after shot peening at 8 bar



clean, bright, satin-finished, without dimensional change or contamination of the parts. The values of roughness obtained after shot peening are shown in Table 8. Three different values of pressure were used on samples with the higher and lower value of  $R_a$  measured. It can be seen that the surface roughness was greatly reduced by shot peening (Fig. 5), and it tends to be improved in proportion with increasing pressure.

#### 4.5 Field emission scanning electron microscope

The effect of different process parameters on the surface roughness of AlSi10Mg parts produced by DMLS was investigated also by FESEM. Looking at Table 8, the samples investigated were the number 15, with parameters very close to the default one for up-skin (rif. Table 1), and the number 3, which showed the best results in terms of  $R_a$  just after construction. As can be seen in Fig. 6, the difference in surface morphology is evident: the sample 3 is clearly smoother than sample 15. It can be assumed that the decrease in hatching distance, together with the lower scanning speed, helps to reduce the presence of voids or necks between the different scanning tracks, leading to a better surface. Also, the effect of shot peening post processing was observed by FESEM. In Fig. 7 are reported the surface morphology of sample 15 and sample 3 after shot peening at 8 bar: it is quite evident the enhancement in surface finishing, reaching a lower value of  $R_a$ . However, it is also clear that the shot peening could not remove the “hills” that form due to processing parameters.

## 5 Conclusions

The effect of some process parameters on the surface roughness of AlSi10Mg parts produced by DMLS was studied with the help of statistical methods. Scan speed was found to have the greatest influence on the surface roughness. The Taguchi method uses S/N ratio to measure the variations of the experimental design. The equation of *smaller-the-better* was selected for the calculation of S/N ratio since it yields the lowest values of surface roughness. It was found that S/N ratio is minimized when

- The scan speed is 900 mm/s,
- The laser power is 120 W,
- The hatching distance is 0.10 mm.

Further, shot peening makes it possible to significantly reduce the surface roughness with glass beads. Different values of pressure were analyzed. The best results were obtained using a pressure of 8 bar ( $R_a$  reduced by up to 83 %). These considerations on laser sintering parameters and the shot peening effect were confirmed by FESEM observations: the images give evidence of the improvement in surface roughness.

## References

1. ASTM (2010) F2792-10e1 Standard terminology for additive manufacturing technologies. ASTM International
2. Chua CK, Leong KF, Lim CS (2003) Rapid prototyping: principles and applications. World Scientific, Singapore
3. Ho HCH, Cheung WL, Gibson I (2002) Effects of graphite powder on the laser sintering behaviour of polycarbonate. Rapid Prototyp J 8:233–242
4. Zhu HH, Lu L, Fuh JYH (2003) Development and characterization of direct laser sintering Cu-based metal powder. J Mater Process Technol 140:314–317
5. Steen WM (1998) Laser material processing, 2nd edn. Springer, London
6. Das S, Fuesting TP, Danyo G, Brown LE, Beaman JJ, Bourell DL (2000) Direct laser fabrication of superalloy cermet abrasive turbine blade tips. Mater Des 21:63–73
7. Hopkinson N, Hague RJM, Dickens PM (2006) Rapid manufacturing: an industrial revolution for the digital age. Wiley, USA
8. Gibson I, Shi D (1997) Material properties and fabrication parameters in selective laser sintering process. Rapid Prototyp J 3 (4):129–136
9. Hao L, Dadbakhsh S, Seaman O, Felstead M (2009) Selective laser melting of a stainless steel and hydroxyapatite composite for load-bearing implant development. J Mater Process Technol 209:5793–5801
10. Chatterjee AN, Kumar S, Saha P, Mishra PK, Choudhury AR (2003) An experimental design approach to selective laser sintering of low carbon steel. J Mater Process Technol 136:151–157
11. Dewidar MM, Lim JK, Dalgarno KW (2008) A comparison between direct and indirect selective laser sintering of metals. J Mater Sci Technol 24(2):227–232
12. Kathuria YP (1999) Microstructuring by selective laser sintering of metallic powder. Surf Coat Technol 116–119:643–647

13. Deckers J, Shahzad K, Vleugels J, Kruth JP (2012) Isostatic pressing assisted indirect selective laser sintering of alumina components. *Rapid Prototyp J* 18(5):409–419(11)
14. Wohler M, Bourell D, Lee G, Beaman J (1996) Production of full density metal-matrix composite by a combined selective laser sintering/metal infiltration process. *Processing and Fabrication of Advanced Materials V*
15. Harlan NR, Bourell D, Park SM, Beaman JJ (2000) Selective laser sintering of zirconia. *Proc. Conf. on Solid Freeform and Additive Fabrication: A Materials Research Society Symposium*
16. Simchi A, Petzoldt F, Pohl H (2003) On development of direct metal laser sintering for rapid tooling. *J Mater Process Technol* 141:319–328
17. Simchi A (2006) Direct laser sintering of metal powders: mechanism, kinetics, and microstructural features. *Mat Sci Eng A* 428:148–158
18. Booyesen GJ, Truscott M, Els J, De Beer DJ (2011) Development of patient-specific implants using direct metal laser sintering in titanium. *Proceedings of the 5th International Conference on Advanced Research in Virtual and Rapid Prototyping, Leiria, Portugal*
19. Delgado J, Ciurana J, Rodríguez CA (2012) Influence of process parameters on part quality and mechanical properties for DMLS and SLM with iron-based materials. *Int J Adv Manuf Technol* 60:601–610
20. Kruth JP, Levy G, Klocke F, Childs THC (2007) Consolidation phenomena in laser and powder-bed based layered manufacturing. *CIRP Ann* 56(2):730–759
21. Dalgarno K (2007) Materials research to support high performance RM parts. *Rapid Manufacturing 2nd International Conference, Loughborough University, 9–12 July: 147–56*
22. Sachdeva A, Singh S, Sharma VS (2012) Investigating surface roughness of parts produced by SLS process. *Int J Adv Manuf Technol*. doi:10.1007/s00170-012-4118-z
23. Song Y (1997) Experimental study of the basic process mechanism for direct selective laser sintering of low-melting powder. *Ann CIRP* 46(1):127–130
24. Masood SH, Rattanawong W, Iovenitti P (2003) A generic algorithm for a best part orientation system for complex parts in rapid prototyping. *J Mater Process Technol* 139(1–3):110–116
25. Byun HS, Lee KH (2006) Determination of the optimal build direction for different rapid prototyping processes using multicriterion decision making. *Rob Comput Integr Manuf* 22(1):69–80
26. Ning Y, Fuh JYH, Wong YS, Loh HT (2004) An intelligent parameter selection system for direct metal laser sintering process. *Int J Prod Res* 42(1):183–199
27. Spierings AB, Herres N, Levy G (2011) Influence of the particle size distribution on surface quality and mechanical properties in AM steel parts. *Rapid Prototyp J* 17(3):195–202
28. Taguchi G (1990) *Introduction to quality engineering*. McGraw-Hill, New York
29. Dingal S, Pradhan TR, Sundar S, Roy Choudhury A, Roy SK (2004) Experimental investigation of selective laser sintering of iron powder by application of Taguchi method. In: *Proceedings of the 2004 Laser Assisted Net Shape Engineering Conference*
30. Yang HJ, Hwang PJ, Lee SH (2002) A study on shrinkage compensation of the SLS process by using the Taguchi method. *Int J Mach Tool Manu* 42:1203–1212
31. Senthilkumaran K, Pandey PM, Rao PVM (2009) Influence of building strategies on the accuracy of parts in selective laser sintering. *Mater Des* 30:2946–2954
32. EOS (2009) *EOSint M 270 User Manual*
33. Ramos JA, Bourell DL, Beaman JJ (2003) Surface over-melt during laser polishing of indirect-SLS metal parts. *Mater Res Soc Symp* 758:53–61
34. Kruth JP, Froyen L, Van Vaerenbergh J, Mercelis P, Rombouts M, Lauwers B (2004) Selective laser melting of iron-based powder. *J Mater Process Technol* 149(1–3):616–622